Simultaneous Dual Echo Gadolinium Enhanced MR-PET for Evaluation of PET Tracer Delivery in Altered Pathophysiology

Gary J Cowin[1]*, Karine Mardon[1], Zachary H. Houston[2,3], Rajiv Bhalla[2], Damion H. R. Stimson[2], Kristofer J. Thurecht[2,3] and Ian M. Brereton[1,2]

[1]National Imaging Facility, Centre for Advanced Imaging, University of Queensland, Brisbane, QLD, Australia, [2]Centre for Advanced Imaging, University of Queensland, Brisbane, QLD, Australia, [3]Australian Institute for Bioengineering and Nanotechnology, ARC Centre of Excellence in Convergent BioNano Science and Technology and ARC Training Centre in Biomedical Imaging Technology, University of Queensland, Brisbane, QLD, Australia

Efficacy of diagnostics and therapeutics for brain tumours can be modulated by vascular delivery and blood brain barrier permeability. Simultaneous dynamic gadolinium MR-PET enables independent assessment of vascular delivery and blood brain barrier integrity in a brain tumour animal model in the presence of a PET tracer.

Dual echo dynamic gadolinium enhanced gradient echo imaging allows simultaneous calculation of T_2* and T_1 images from the TE image pairs. Relaxivity values then enabled determination of independent T_2*- and T_1-derived gadolinium concentrations simultaneously with measurement of [18F]DPA-714 neuroinflammation radiotracer delivery.

Separate T_2*- and T_1-derived gadolinium concentrations curves were derived in a selection of tumours and normal tissue, reflecting vascular delivery and tissue uptake. Changes in the PET activity curves were seen in tumours and normal tissue, reflecting changes in the MR derived dynamic curves. The dramatic changes in the MR-derived vascular delivery and tissue uptake estimates may improve the understanding of the alteration of delivery and uptake of new theranostic agents.

Keywords: MR-PET, gadolinium contrast agents, PET tracer delivery, T2*, T1, blood brain barrier

INTRODUCTION

The measured activity of a diagnostic or therapeutic positron emission tomography (PET) tracer can be modulated by vascular delivery, transport into and out of the tissue, specific and non-specific binding of the radiotracer and metabolism, particularly in the brain where the blood brain barrier (BBB) strongly regulates transport from the vasculature to the neural tissue [1]. Tumour growth is accompanied by neovascular development and compromised BBB integrity. These effects can dramatically change the transport of candidate diagnostics and therapeutics and contribute to the effectiveness of new treatments, with recent data demonstrating that nanomedicine accumulation is related to vascular leakiness, rather than tumour volume alone [2].

Kinetic analysis of PET tracers requires determination of the time dependent change in tracer activity in the blood (input function). This is challenging in rodents, particularly mice, as methods

often require blood sampling and/or surgical procedures, and imaging methods are limited by the low resolution of PET [3]. The higher spatial and temporal resolution of magnetic resonance imaging (MRI) has potential to allow MR image derived arterial input function (AIF) for PET pharmacokinetic modelling [4].

The change in MR image intensity during contrast-enhanced magnetic resonance imaging (MRI) is not linearly related to the Gadolinium (Gd) concentration over a large concentration range, particularly when the image contrast is a mix of T1, T2 and/or T2* weighting. For comparison, in nuclear imaging methods like PET, the image intensity observed is in units of radioactivity that are directly related to the activity of tracer present. Lower concentrations of Gd produces T_1 shortening resulting in signal enhancement in T_1 weighted images, as used in dynamic contrast enhanced (DCE) MRI [5]. For higher Gd concentrations, T_2 and T_2^* shortening dominate, decreasing the signal, ultimately nulling at high concentrations, as exploited in dynamic susceptibility (DSC) MRI [6]. Typically, imaging sequences are optimised for only one contrast, T_1 or T_2^*, dependent on the type of perfusion regime being investigated [7]. Dual echo gradient echo MRI enables T_1 and T_2^* changes to be calculated simultaneously [8]. Therefore, we move from acquiring separate T_1 or T_2^* contrast images to simultaneously calculating T_1 and T_2^* images from gradient echo image pairs with TE = 3 and 6 ms. This allows parallel changes in vascular delivery and tissue uptake to be determined, which was not possible previously.

The aim of this study was to demonstrate independent measurement of MR derived vascular delivery and tissue uptake simultaneously with the PET tracer [18F]DPA-714 [9] in a mouse model of glioblastoma. This was demonstrated using a selection of mice with glioblastoma tumours at different stages of progression.

MATERIALS AND METHODS

Animal Model and Preparation

The mouse model of spontaneous developing glioblastoma was sourced from a colony at the Queensland Brain Institute, University of Queensland. The model was prepared by crossing Gt(ROSA)26So$^{rtm14(CAG-tdTomato)Hze}$ 20023653 with Pten^{tm2MAK}; Rb1^{tm2Brn}; Trp53^{tm1Brn}; Tg(GFAP-cre/Esr1*,- lacZ)BSbk (alleles) and backcrossed six generations to latter mice to generate the high grade glioma mouse model [2, 10]. All experiments were approved by the University of Queensland Animal Ethics Committee and followed the Australian Code of Practice for Use of Animals for Scientific Purposes (AIBN/142/19/UQ).

Anaesthetised mice were cannulated in the tail vein using 55 cm of tygon tubing (ID 0.01 inch, OD 0.03 inch) with just the metal needle from a 30G needle on one end and an inserted 30G needle on the other end. Imaging was performed with a combined MR-PET system, comprising a 300 mm bore 7T ClinScan MR scanner (Bruker, Germany), running Siemens VB17, with a removable PET insert (Bruker, Germany) containing 3 rings of 16 detector blocks with 15 × 15 LSO crystals (1.6 × 1.6 × 10 mm) per block, located at the centre of the magnet bore. The scanner was operated under Siemens Inveon Acquisition Workplace
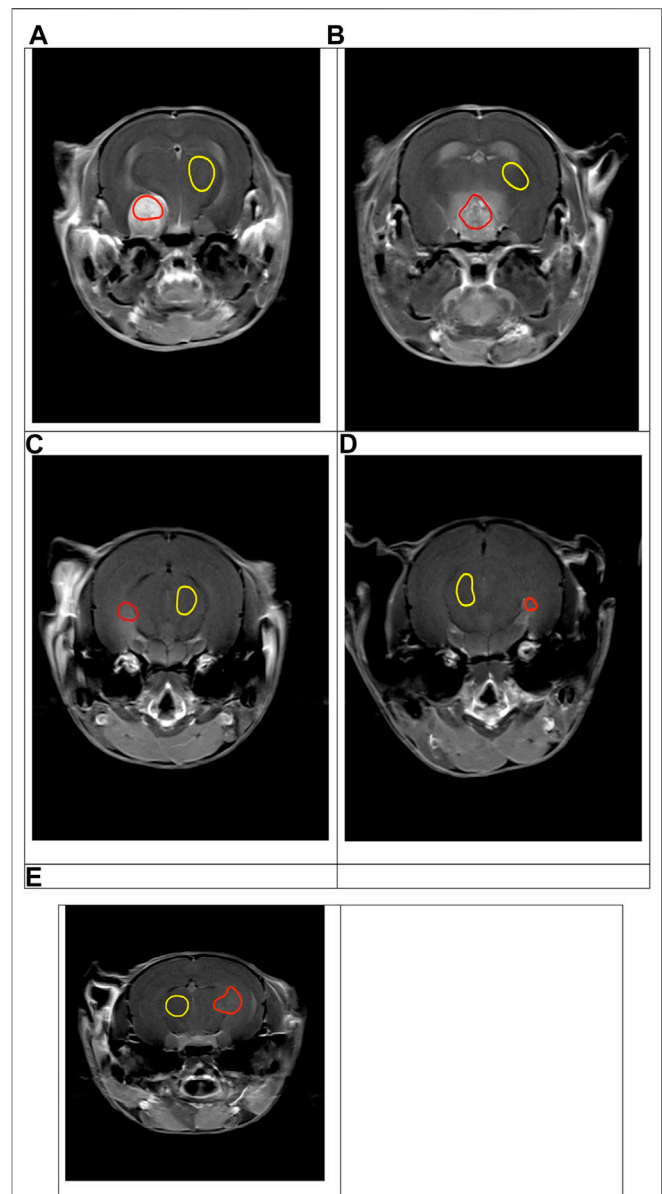
FIGURE 1 | T$_1$_TSE_Tra images showing variable tumour growth and gadolinium enhancement in the tumour (red ROI) and in the thalamus (yellow ROI) for mouse 1-5, **(A–E)** respectively.

(IAW, version 1.5.0.28). The animal was placed on an animal bed warmed with recirculating water and a 23 mm ID MRI RF coil inside the PET ring was used to acquire MR images simultaneously with the PET acquisition. A single syringe was prepared and connected to the cannula containing approximately 10 MBq of [18F]DPA-714 [9] tracer solution, 50 μL Gadovist (Bayer, Germany) and saline/10% ethanol to give a total volume of 200 μL.

MR-PET

Following MRI localiser images, a 60 min PET acquisition was started simultaneously with dynamic spoiled gradient echo (GRE)

FIGURE 2 | Gadovist thalamus derived concentration derived from the changes in: **(A)** T_2^*; **(B)** T_1; **(C)** thalamus time activity curve representing the uptake of [18F] DPA-714 as standard uptake value normalised to body weight (SUV-BW). Mouse 1-red, mouse 2-green, mouse 3-blue, mouse 4 black and mouse 5-purple.
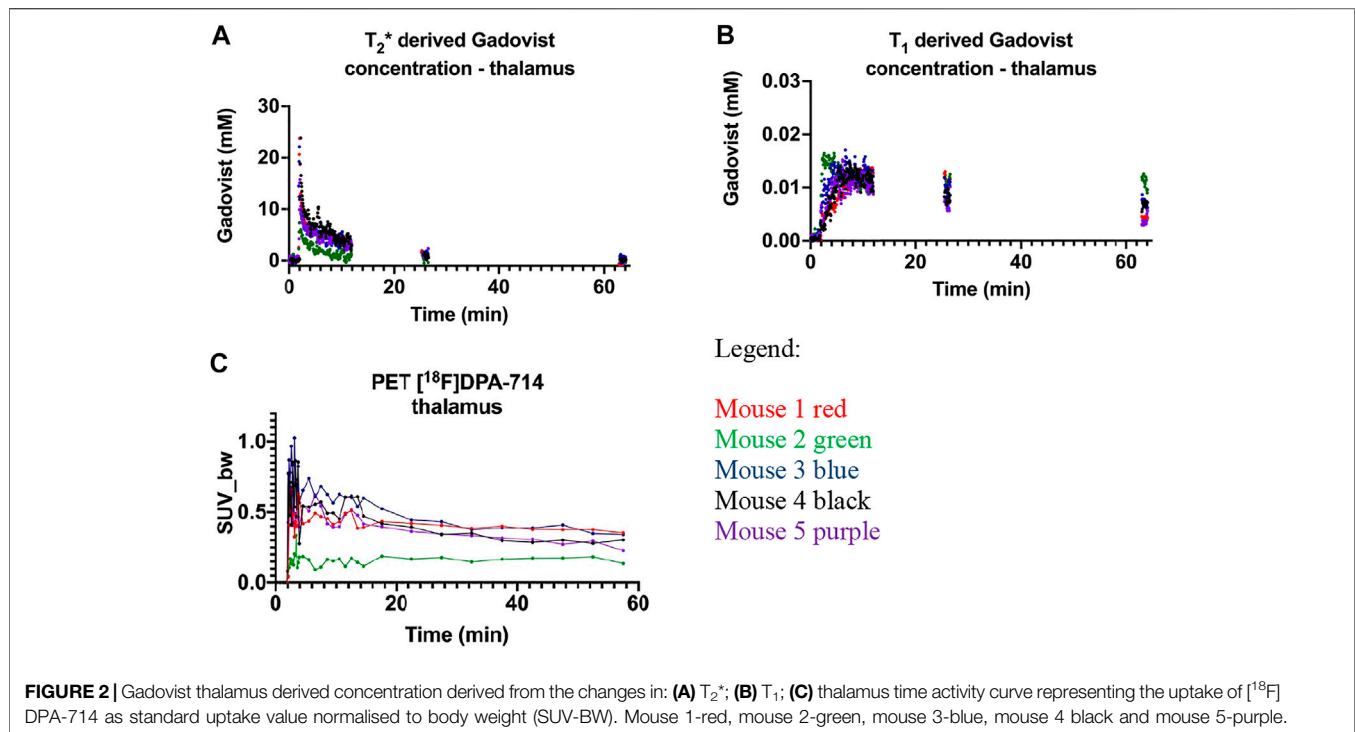
image acquisition with the following parameters: pulse angle = 45°, 6 × 1 mm slices, FOV = 20 × 20 mm, in-plane resolution = 313 × 313 μm, TR = 75 ms, TE = 3 and 6 ms, acquisition time = 3.6 s, 200 measurements. After a 2 min baseline period the combined PET tracer and Gadovist solution was injected by hand over approximately 5 s, with no flush.

Following the dynamic GRE images, high resolution transverse and sagittal T_2 turbo spin echo (TSE) anatomical images were acquired with the following parameters: 19 × 0.6 mm slices, FOV = 25 × 18.74 mm, in-plane resolution = 98 × 98 μm, TR = 2,200 ms, TE = 35 ms, averages = 2, acquisition time = 4:11 and then coronal with the following parameters: 23 × 0.6 mm slices, FOV = 20 × 20 mm, in-plane resolution = 104 × 104 μm, TR = 2,650 ms, TE = 35 ms, averages = 2, acquisition time = 5:02. Another block of 20 GRE dynamic measurements was then acquired.

Next, anatomical transverse and sagittal T_1 weighted TSE images with the following parameters: 19 × 0.6 mm slices, FOV = 19 × 18.74 mm, in-plane resolution = 78 × 78 μm, TR = 600 ms, TE = 13 ms, turbo factor = 7, averages = 3, acquisition time = 5:21 and coronal images with parameters: 25 × 0.6 mm slices, FOV = 25 × 20.75 mm in-plane resolution = 78 × 78 μm, TR = 600 ms, TE = 13 ms, turbo factor = 7, averages = 3, acquisition time = 8:07 were acquired with the same geometric positioning as the T_2 TSE images.

Following acquisition of fl3d_swi and fl3d_dixon images (not reported in this paper), a final set of 20 GRE dynamic measurements was then acquired. Therefore, dynamic scans extended for 60 min post injection.

At the end of the imaging, the cannula radioactivity was measured and decay corrected to allow calculation of the

injected dose. PET data was reconstructed using a dedicated PET reconstruction software developed by the University of Tübingen. PET images with a matrix of 89 × 128 × 128 and field-of-view = 68 × 90 × 90 mm were reconstructed using the ordered-subset expectation maximization (OSEM2D) algorithm with 3 × 30 s, 15 × 10 s, 11 × 60 s and 9 × 300 s time frames for 60 min. MRI and PET datasets were aligned using Siemens Inveon Research Workplace (IRW, version 4.2.0.8) software employing a standard transformation matrix.

Image Processing

HOROS (www.horosproject.org) was used for MRI region-of-interest (ROI) drawing and output. On the central slice of the tumour, one ROI was positioned within tumour tissue taking care to avoid the susceptibility effect at the edge of the brain. The high resolution T_1 and T_2 image sets were used for placement of the tumour ROIs. The tumours with low enhancement on the T_1 images (**Figures 1C–E**) were more easily visualised on the T_2 TSE images. The ROI placements were then checked on the TE = 6 ms images, both before and after Gd injection, to ensure the ROI regions of the images were not distorted due to susceptibility effects. A second ROI was positioned in the thalamus to represent normal brain tissue (**Figure 1**). The ROIs were then propagated to all time point images, exported as csv files and imported into excel for calculations.

Calculation of the gadolinium concentration derived independently from T_2^* and T_1 time changes were determined from equations modified as previously described [8], using TE1 = 3 ms and TE2 = 6 ms, TR = 75 ms, pulse angle = 45°, r2* = 6.35 s^{-1} mM^{-1} and r1 = 6.1 s^{-1} mM^{-1} (Gadovist solutions at

7.0 T), A = mean ROI intensity (TE = 3 ms) and B = mean ROI intensity (TE = 6 ms), $M_o sin\alpha$ = 2,700.

The T_2^* was calculated using:

$$T_2^* = \frac{TE1}{Ln\left(\frac{A}{B}\right)}$$

The T_2^* derived concentration was then calculated using:

$$T_2^* \; concentration = \left(\frac{1}{T_2^*} - \frac{1}{T_{2baseline}^*}\right) \div r2^*$$

The baseline values were determined by averaging data points 3–12 during the baseline period before the Gd injection.

The T_1 was calculated for TE = 3 and 6 ms image pairs using the following equations:

$$D = 1 - \frac{A \times \left(\frac{A}{B}\right)}{M_o \times sin \propto}$$

$$T_1 = 1 \div \left(TR \div \left(\frac{D}{D \times cos \propto}\right)\right)$$

The T_1 derived concentration was then calculated using:

$$T_1 \; concentration = \left(\frac{1}{T_1} - \frac{1}{T_{1baseline}}\right) \div r1$$

The **Appendix** contains the equations expressed in a form that can be pasted into excel to perform the calculations from TE = 3 ms and TE = 6 ms image pairs. The values were then expressed as change from the baseline and 3 point floating averaging was applied.

Prism 8 software (GraphPad Software, United States) was used for plotting the data.

RESULTS

Tumour Growth and Enhancement

Spontaneous brain tumours 5 months post induction displayed variable size and T_1 gadolinium enhancement (**Figure 1**). Similar to tumour growth in humans, the model was extremely heterogenous in growth rates and not all animals produced a tumour. The tumours produced included a large tumour with strong Gd enhancement (**Figure 1A**), a large tumour with reduced Gd enhancement (**Figure 1B**), and three slow growing tumours with weak Gd enhancement (**Figures 1C–E**). The T_2 weighted images provided easier visualisation of the tumours with weak enhancement. This allowed the potential of the dual echo method to measure changes in physiology during tumour growth to be assessed.

Normal Tissue

Firstly, we compared Gd and PET data from the thalamus region as control tissue in all mice. A rapid initial increase and subsequent decrease in the T_2^*-derived Gadovist concentration (**Figure 2A**) is consistent with vascular Gd bolus passing through the tissue and then equilibrating throughout the total blood volume. The slower uptake and gradual decrease observed in

the T_1-derived Gadovist concentration curve (**Figure 2B**) is consistent with Gadovist crossing the BBB and entering the brain tissue [5]. [^{18}F]DPA-714 thalamus time activity curve (TAC) displayed a rapid increase followed by a decrease (**Figure 2C**) in activity. Plots were consistent for mice 1, 3, 4 and 5 with lower T_2^* and TAC curves for mouse 2.

Poor Injection

The T_2^* concentration curve for mouse 2 was below the other four animals (**Figures 2A, 3E**, green data). Increased resistance during intravenous dose injection was noted, consistent with poor cannulation and the solution entering the tail tissue instead of the tail vein. This illustrates the power of the T_2^* derived Gd concentration to ensure cannulation consistency in group studies where animals with decreased agent delivery can be excluded from further analysis. The decreased Gd delivery to the normal tissue was also reflected in the decreased activity of the PET tracer activity curve (**Figure 2C**), illustrating the parallel changes in both Gd and PET dynamic tracer injection. The PET dynamic curve of mouse 2 was flat compared to the decrease in intensity post bolus of the other mice consistent with slow release of the tracer injected into the tail tissue, rather than the vein. The T_1 derived Gd concentrations curves (**Figure 2B**) reflect tissue uptake of Gd and were grouped together. This is consistent with the intact blood brain barrier restricting transport of the Gadovist from the blood into the brain tissue. The reduced vascular delivery in mouse 2 did not appear to alter the normal tissue uptake of Gadovist. The decreased intensity of the Gd and PET tracer curves in the normal tissue of mouse 2, was not exhibited in the tumour tissue of mouse 2, as discussed below.

Tumour Tissue

The tumour tissue in mice 1 and 2 both displayed dramatically enhanced T_2^* (**Figure 3A**) and T_1 (**Figure 3B**) derived concentration curves relative to corresponding thalamus curves (**Figures 2A,B**) and compared to the tumour tissue in mice 3, 4, and 5. Mice 3, 4 and 5 showed modest increases in T_2^* and T_1 derived concentrations in the tumours (**Figure 3C**) compared to the normal thalamus tissue (**Figure 3E**).

The extent of the dramatic increase of delivery and uptake of Gadovist in the two large tumours was not evident in the time activity curves representing the tumour uptake of [^{18}F]DPA-714 (**Figure 3F**). For example, at 10 min the T2* curve for the tumour in mouse 2 is approximately 8 times the other curves (**Figure 3A**), yet the TAC curve is only about double the other curves (**Figure 3F**). The TAC for the tumour in mouse 2 was similar in intensity to the other three tumours (**Figure 3F**), despite a higher bolus (**Figure 3A**) and the TAC amplitude being of less than half the intensity in the thalamus compared to the other mice.

DISCUSSION

Gd enhanced MRI typically follows changes in image contrast using standard T_1, T_2 or T_2^* contrast. Dual echo imaging progresses this to calculation of unique gadolinium
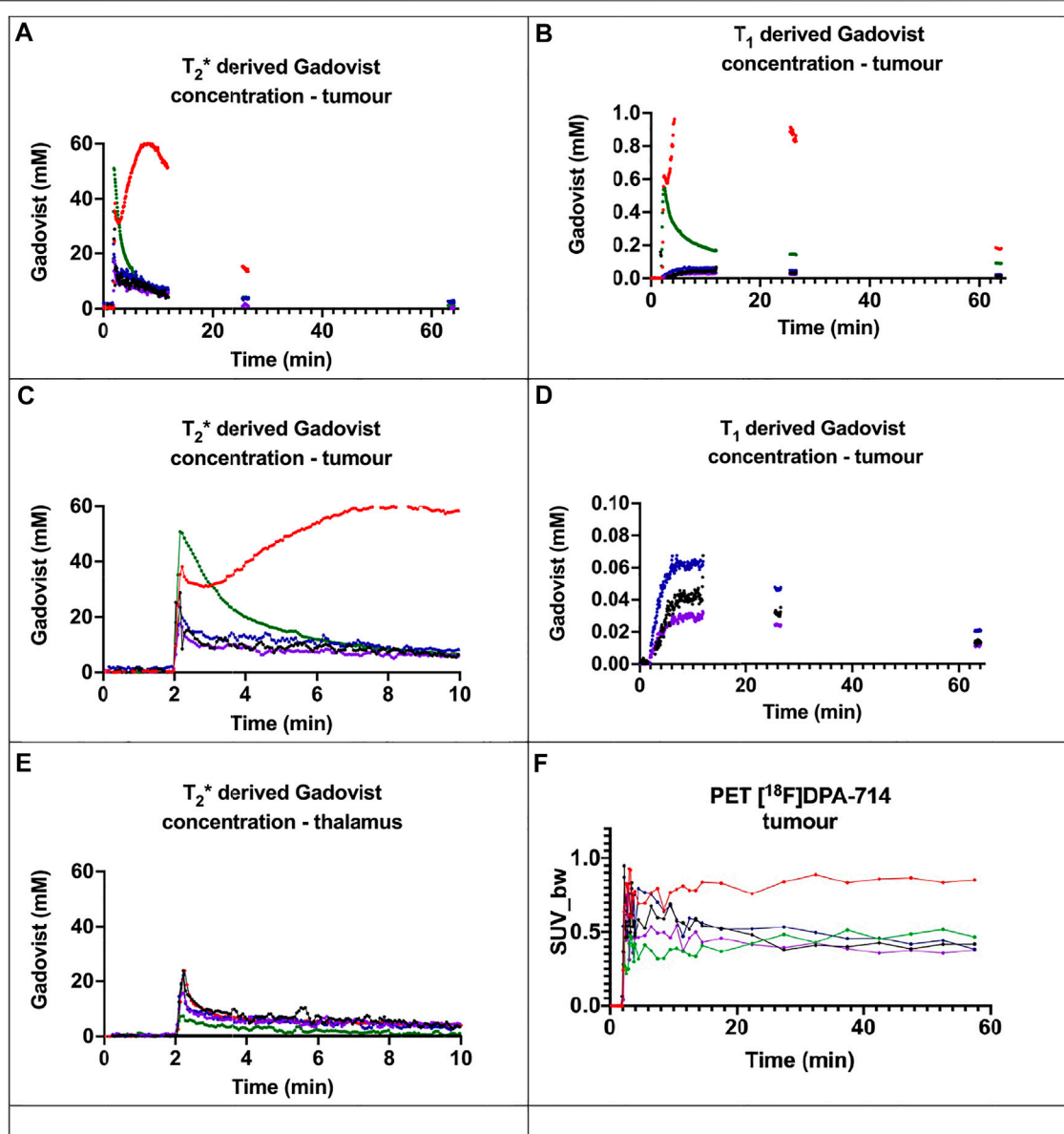
FIGURE 3 | Gadovist concentration derived from the changes in: **(A)** T_2^*; **(B)** T_1; **(C)** first 10 min of T_2^* derived Gadovist concentration in the tumour **(D)** expanded scale of T_1 derived Gadovist concentration of mice 3, 4, and 5; **(E)** first 10 min of T_2^* derived Gadovist concentration in the thalamus **(F)** tumour time activity curve for [^{18}F]DPA-714. For mouse 1 in **(B)**, the maximum calculated value was ~5,000 nmol, above which the calculation failed. Mouse 1-red, mouse 2-green, mouse 3-blue, mouse 4 black and mouse 5-purple.

concentrations from T_1 and T_2^* changes with time. This can provide novel insights into differences in the vascular delivery and BBB permeability as demonstrated in the spontaneous developed brain tumours. Changes in T_2^* and T_1 were independently determined from images acquired with two TE values. The resulting relaxivity values were used to calculate the concentration derived from the T_2^* and T_1 values. Using these data, the tumours in mice 1 and 2 showed dramatically enhanced vascular delivery and tissue uptake of Gadovist. The tumours in mice 3, 4 and 5 illustrated moderately increased delivery and tissue uptake of Gadovist.

The choice of TE values is dependent on the concentration of Gd used and expected changes in Gd uptake. A larger difference in TE values makes the procedure more sensitive to changes in T_2^* changes. However, increased TE values result in stronger magnetic susceptibility effects and image distortion, particularly at brain boundaries near air cavities. Depending on the MR system capability, a pair of shorter TE values may be beneficial, particularly for mice. Larger animals may be suitable for longer TE values and a lower Gd volume compared to blood volume. The temporal resolution of 3.6 s provided approximately 4 data points to define the initial increase of the bolus. Both increasing

the image resolution or number of slices decreases the temporal resolution.

The determination of localised arterial input function from vascular $T_2^\star$ derived concentrations would allow PET parametric calculations [4] for specific tissue or region of interest [11]. To achieve this goal, *in vivo* determination of the Gadovist relaxivity values is required, rather than solution-derived values, as used in this study. MR-PET allows simultaneous quantification of a MR contrast agent and a PET surrogate e.g., using copper-64 [12, 13] or Yttrium-68 [14], as the gold standard for *in vivo* quantification. Initial reports indicate *in vivo* relaxivity values are lower than in solution [15]. MR-PET can be used to gain a greater understanding of how the relaxivity values change in the different organs and under different pathological conditions. This is critical for accurate quantification of gadolinium contrast agent concentrations *in vivo*. Targeted MR-PET experiments are required to investigate relaxivity values and concentration linearity in normal and pathological tissue. This will greatly improve the quantitative potential of MRI measurements.

The calculation of the two T_1 and $T_2^\star$ concentrations from the TE image pairs allows altered tissue haemodynamics and perfusion to be measured within the tissue, not in a remote vessel. Subtle BBB transport changes are discernible from T_1 changes, as observed for mice 3–5 (**Figure 3D**). Areas of extreme extravasation [16], mouse 1, are indicated by $T_2^\star$ changes. Ischaemia, blocking tracer delivery, or hyperperfusion can be easily assessed by MRI.

Despite being simultaneously injected from a single syringe, the very large changes in Gd tumour delivery and uptake were not mirrored with the PET tracer tested in these pilot animals. Future experiments, incorporating blocking studies or cold washout are required to better understand the consequences of the changes in MR derived delivery and tissue uptake upon accumulation of the PET tracers, particularly in pathological tissue as illustrated by mice 1 and 2. The structural difference of Gadovist and DPA714 may also contribute to the differences observed between the MR and PET dynamic curves. Future experiments with structurally similar or identical MR contrast agents and PET tracers are also required to understand this observation.

As the Gd enhanced MR measures are non-targeted, this may also enable unique insights into non-specific uptake of PET tracers. Larger studies are required to investigate the reproducibility of the results and how the methodology, including Gd concentrations and acquisition parameters

modulates the calculation of the T_1 and $T_2^\star$ derived concentrations.

CONCLUSION

Simultaneous dual echo MR-PET was shown to enable parallel and independent estimation of vascular ($T_2^\star$ derived) and tissue (T_1 derived) concentration curves for Gadovist in mice. This allows greater temporal resolution for both parameters, which would normally be determined with separate T_1 or $T_2^\star$ contrast image sets. This approach can be developed further to improve the understanding of pathological changes in tissue and how this affects theranostic and PET tracer accumulation for neurological studies.

DATA AVAILABILITY STATEMENT

The raw data supporting the conclusion of this article will be made available by the authors, without undue reservation.

ETHICS STATEMENT

The animal study was reviewed and approved by University of Queensland.

AUTHOR CONTRIBUTIONS

All authors designed the study. GC, KM and ZH performed the imaging experiments. RB and DHRS performed the radiochemistry. GC performed the analysis of the data and drafted the paper with review by all authors.

ACKNOWLEDGMENTS

REFERENCES

1. Pike VW. PET Radiotracers: Crossing the Blood-Brain Barrier and Surviving Metabolism. *Trends Pharmacol Sci* (2009) 30(8):431–40. doi:10.1016/j.tips.2009.05.005

2. Houston ZH, Bunt J, Chen K-S, Puttick S, Howard CB, Fletcher NL, et al. Understanding the Uptake of Nanomedicines at Different Stages of Brain Cancer Using a Modular Nanocarrier Platform and Precision Bispecific Antibodies. *ACS Cent Sci* (2020) 6(5):727–38. doi:10.1021/acscentsci.9b01299

3. Laforest R, Sharp TL, Engelbach JA, Fettig NM, Herrero P, Kim J, et al. Measurement of Input Functions in Rodents: Challenges and Solutions. *Nucl Med Biol* (2005) 32:679–85. doi:10.1016/j.nucmedbio.2005.06.012

4. Poulin E, Lebel R, Croteau E, Blanchette M, Tremblay L, Lecomte R, et al. Conversion of Arterial Input Functions for Dual Pharmacokinetic Modeling Using Gd-DTPA/MRI and 18 F-FDG/PET. *Magn Reson Med* (2013) 69(3):781–92. doi:10.1002/mrm.24318

5. Jain R. Measurements of Tumor Vascular Leakiness Using DCE in Brain Tumors: Clinical Applications. *NMR Biomed* (2013) 26(8):1042–9. doi:10.1002/nbm.2994

6. Willats L, Calamante F. The 39 Steps: Evading Error and Deciphering the Secrets for Accurate Dynamic Susceptibility Contrast MRI. *NMR Biomed* (2013) 26(8):913–31. doi:10.1002/nbm.2833

7. Jahng G-H, Li K-L, Ostergaard L, Calamante F. Perfusion Magnetic Resonance Imaging: a Comprehensive Update on Principles and Techniques. *Korean J Radiol* (2014) 15(5):554–77. doi:10.3348/kjr.2014.15.5.554

8. Kuperman VYU, Karczmar GS, Blomley MJK, Lewis MZ, Lubich LM, Lipton MJ. Differentiating between T1 and T2* Changes Caused by Gadopentetate Dimeglumine in the Kidney by Using a Double-echo Dynamic MR Imaging Sequence. *J Magn Reson Imaging* (1996) 6(5):764–8. doi:10.1002/jmri.1880060509

9. James ML, Fulton RR, Vercoullie J, Henderson DJ, Garreau L, Chalon S, et al. DPA-714, a New Translocator Protein-specific Ligand: Synthesis, Radiofluorination, and Pharmacologic Characterization. *J Nucl Med* (2008) 49(5):814–22. doi:10.2967/jnumed.107.046151

10. Chow LML, Endersby R, Zhu X, Rankin S, Qu C, Zhang J, et al. Cooperativity within and Among Pten, P53, and Rb Pathways Induces High-Grade Astrocytoma in Adult Brain. *Cancer Cell* (2011) 19(3):305–16. doi:10.1016/j.ccr.2011.01.039

11. Calamante F. Arterial Input Function in Perfusion MRI: a Comprehensive Review. *Prog Nucl Magn Reson Spectrosc* (2013) 74:1–32. doi:10.1016/j.pnmrs.2013.04.002

12. Uppal R, Catana C, Ay I, Benner T, Sorensen AG, Caravan P. Bimodal Thrombus Imaging: Simultaneous PET/MR Imaging with a Fibrin-Targeted Dual PET/MR Probe-Feasibility Study in Rat Model. *Radiology* (2011) 258(3):812–20. doi:10.1148/radiol.10100881

13. Kim H, Lee S-J, Davies-Venn C, Kim JS, Yang BY, Yao Z, et al. 64Cu-DOTA as a Surrogate Positron Analog of Gd-DOTA for Cardiac Fibrosis Detection with PET. *Nucl Med Commun* (2016) 37(2):188–96. doi:10.1097/mnm.0000000000000417

14. Le Fur M, Rotile NJ, Correcher C, Clavijo Jordan V, Ross AW, Catana C, et al. Yttrium-86 Is a Positron Emitting Surrogate of Gadolinium for Noninvasive Quantification of Whole-Body Distribution of Gadolinium-Based Contrast Agents. *Angew Chem Int Ed* (2020) 59(4):1474–8. doi:10.1002/anie.201911858

15. Rohrer M, Bauer H, Mintorovitch J, Requardt M, Weinmann H-J. Comparison of Magnetic Properties of MRI Contrast media Solutions at Different Magnetic Field Strengths. *Invest Radiol* (2005) 40(11):715–24. doi:10.1097/01.rli.0000184756.66360.d3

16. Bjornerud A, Sorensen AG, Mouridsen K, Emblem KE. T1- and T*2-Dominant Extravasation Correction in DSC-MRI: Part I-Theoretical Considerations and Implications for Assessment of Tumor Hemodynamic Properties. *J Cereb Blood Flow Metab* (2011) 31(10):2041–53. doi:10.1038/jcbfm.2011.52

Conflict of Interest: The authors declare that the research was conducted in the absence of any commercial or financial relationships that could be construed as a potential conflict of interest.

Publisher's Note: All claims expressed in this article are solely those of the authors and do not necessarily represent those of their affiliated organizations, or those of the publisher, the editors and the reviewers. Any product that may be evaluated in this article, or claim that may be made by its manufacturer, is not guaranteed or endorsed by the publisher.

APPENDIX

Calculation of dual echo, using TE = 3 and 6 ms, T2*, T1 and $T_2^\star$ and T_1 derived Gadovist concentration in excel:

    The following equations can be copied and pasted into excel to calculate the gadolinium concentrations where A = intensity for TE = 3 ms ROI and B = intensity for TE = 6 ms ROI and the parameters listed in the methods. These equations can only be applied when TE2 is twice TE1, e.g., using TE2 = 6 ms and TE1 = 3 ms. The baseline values were determined by averaging data points 3-12 during the baseline period before the Gd injection.

T_2^* calculations:

$$T_2^* = 3/LN\,(A/B)\,T_2^* \text{ derived gadovist concentration}$$
$$= \left(\left(1/\left(T_2^*/1000\right) - \left(1/\left(T_2^*/1000\right)\right)\right)/6.35\right)$$

Where 6.35 $s^{-1}\,mM^{-1}$ equals the T_2^* relaxivity determined at 7T determined on the 7T Clinscan used in the study. The 1,000 converts ms to s to match the units of the relaxivity.

T_1 calculations:

$$T_1 = ABS\left(75/\left(LN\left(\left(1 - (A*(A/B)/C)\right)/\left(1 - (A*(A/B)\right.\right.\right.\right.$$
$$\left.\left.\left.\left. \times /C*0.707\right)\right)\right)\right)$$

Where C = $M_o \sin\alpha$ = 2,700.

$$M_o = Ae/\left(\left(1 - EXP\left(-TR/T_1\right)\right)/\left(1 - COS\,(\alpha)*EXP\left(\right.\right.\right.$$
$$\left.\left.\left. - TR/T_1\right)\right)*SIN\,(\alpha)*EXP\left(-TE/T_2^*\right)\right)$$

Where Ae is the average baseline intensity and we used baseline brain values of T_1 = 2000 ms, and $T_2^\star$ = 40 ms

$$T_1 \text{ derived Gadovist concentration}$$
$$= \left(\left(1/\left(T_1/1000\right) - \left(1/\left(T_{1\,baseline}/1000\right)\right)\right)/6.1\right)$$

Where 6.1 $s^{-1}\,mM^{-1}$ equals the T_1 relaxivity determined at 7T determined on the 7T Clinscan used in the study. The 1,000 converts ms to s to match the units of the relaxivity.